Biochemical and Biophysical Research Communications 457 (2015) 398–403

Contents lists available at ScienceDirect

Biochemical and Biophysical Research Communications

journal homepage: www.elsevier.com/locate/ybbrc

Structural and biochemical characterization of MCAT from photosynthetic microorganism *Synechocystis* sp. PCC 6803 reveal its stepwise catalytic mechanism

Yinghui Liu [a], Yanbin Feng [a], Yayue Wang [a, b], Xia Li [c], Xupeng Cao [a], Song Xue [a, *]

[a] Marine Bioengineering Group, Dalian Institute of Chemical Physics, Chinese Academy of Sciences, Dalian 116023, China
[b] University of Chinese Academy of Sciences, Beijing 100039, China
[c] Dalian Polytechnic University, Dalian 116034, China

ARTICLE INFO

Article history:
Received 14 December 2014
Available online 9 January 2015

Keywords:
MCAT
Synechocystis sp. PCC 6803
Structure
Intermediate

ABSTRACT

Malonyl-coenzyme A: acyl-carrier protein transacylase (MCAT) catalyzes the transfer of malonyl group from malonyl-CoA to the holo-acyl carrier protein (Holo-ACP), yielding malonyl-ACP. The overall reaction has been extensively studied in heterotrophic microorganisms, while its mechanism in photosynthetic autotrophs as well as the stepwise reaction information remains unclear. Here the 2.42 Å crystal structure of MCAT from photosynthetic microorganism *Synechocystis* sp. PCC 6803 is presented. It demonstrates that Arg113, Ser88 and His188 constitute catalytic triad. The second step involved ACP-MCAT-malonyl intermediate is speed-limited instead of the malonyl-CoA-MCAT intermediate in the first step. Therefore His87, Arg113 and Ser88 render different contributions for the two intermediates. Additionally, S88T mutant initializes the reaction by H87 deprotonating S88T which is different from the wild type.

1. Introduction

Malonyl-CoA: acyl-carrier protein transacylase (MCAT) encoded by *fabD* transfers malonyl group from malonyl-CoA to the holo-acyl carrier protein (Holo-ACP) forming malonyl-ACP, the key building block for fatty acid and aromatic polyketides biosynthesis in microorganisms. Therefore MCAT draws a lot of attention as one of the most promising targets to inhibit or kill *Mycobacterium tuberculosis* and other lethal bacteria [1,2]. Recently, cyanobacteria are attractive hosts for biofuel production as they can convert CO_2 and sunlight directly into organic compounds (e.g. lipids) which can be the potential resource of carbon-based biofuels [3–5]. Since fatty acid is also an indispensable component of photosynthetic apparatus in photosynthetic autotrophs, its biosynthesis plays a pivotal role in the photoautotrophic growth and lipid accumulation in cyanobacteria. It was demonstrated that the over-expressed *fabD* gene in *Brassica napus*, *Arabidopsis* and *Saccharomyces cereviseae* obviously increased the lipid content [6,7], which provided an approach to enhance fatty acid synthesis of cyanobacteria by manipulation of MCAT expression. In order to further understand the lipid accumulation, the fundamental information on the catalytic mechanism of MCAT from cyanobacteria is required. So far, structural information on MCAT is only available in certain heterotrophic species, including *Escherichia coli*, *Streptomyces coelicolor*, *Helicobacter pylori*, *M. tuberculosis*, *Staphylococcus aureus*, *Streptococcus pneumonia* and *Xanthomonas oryzae* pv. *oryzae* etc. [8–13], and three potential catalytic mechanisms have been reported, which are sharing similar but not identical molecular process, while the structure and catalytic mechanism of MCAT in cyanobacteria is unknown.

Here the crystal structure of MCAT from cyanobacteria *Synechocystis* sp. PCC 6803 (SpMCAT) was studied, and the functions of relevant conserved amino acids residues in MCAT had been explored by mutagenesis. Structure and mutagenesis study demonstrate that His87, Ser88 and Arg113 contribute crucial roles in the ACP-MCAT-malonyl intermediate, which may be speed-limited in the catalytic process.

2. Material and methods

2.1. Expression and purification of SpMCAT and SpACP

The SpMCAT was overexpressed, purified, and crystallized as described previously [14]. The ACP of *Synechocystis* sp. PCC 6803

* Corresponding author. Fax: +86 411 84379069.
E-mail address: xuesong@dicp.ac.cn (S. Xue).

http://dx.doi.org/10.1016/j.bbrc.2015.01.003
0006-291X/

was cloned and ligated into pET28a. The plasmid containing the ACP was transferred into the host strain BAP1 which contained a chromosomal insertion of the *Bacillus subtilis Sfp* gene [15]. Then the ACP was overexpressed in the holo form by post transcriptional modification, with induction by 0.5 mM IPTG at 37 °C for 3 h. The cells were harvested by centrifugation (6000 rpm, 20 min) and stored at −80 °C until they were used. The purification method of holo-ACP was similar to SpMCAT with minor modification. The FPLC buffer of Holo-ACP was 25 mM Tris–HCl (pH 7.5), 2 mM DTT, 5% glycerol and 100 mM NaCl. Lastly the protein was concentrated with Amicon centriprep concentrator 10 KDa (Millipore), and stored at −80 °C until it was used.

2.2. Structure determination of SpMCAT

Crystallization, data collection and processing of SpMCAT were described previously [14]. The structure was solved by molecular replacement using Phaser [16] from the CCP4 suite [17] with MCAT of *E. coli* (PDB: 1MLA) as a search model. After one round of rigid-body refinement with Phenix [18], manual rebuilding was performed in Coot [19]. Subsequently, further rounds of restrained refinement were performed and water molecules were added and adjusted. Figures containing protein structures were generated with PyMol (*www.pymol.org*) and Chimera [20]. Sequence comparison was generated by ESPript 3.0 [21]. The structural information of SpMCAT is available in PDB database (PDB: 4RR5).

2.3. Construction of SpMCAT mutants

The mutant primers were designed by DNA Man and summarized in Supplementary Table 1. Mutations of SpMCAT were performed with the Prime Star Mix (TaKaRa) according to the manufacturer's instructions and verified by sequencing. The plasmids were transferred to *E. coli* BL21 (DE3). Expression and purification conditions were the same as that of the wild type SpMCAT.

2.4. Coupled enzymatic assay

The enzymatic activities of SpMCAT and mutants were detected following the previously reported α-ketoglutarate dehydrogenase (KDH)-coupled assay system [22] with minor modification. Briefly, KDH-dependent consumption of coenzyme A (CoA) generated by MCAT is accompanied by a reduction of nicotinamide adenine dinucleotide (NAD^+) to NADH and the rate of NADH production was measured via spectrometry at the wavelength of 340 nm using a UV Spectrometer (JASCO Corporation, Tokyo, Japan). The final concentrations of the reaction mixture were 50 mM phosphate buffer (pH 6.8), 1 mM EDTA, 0.1 mg/ml BSA, 1 mM DTT, 2 mM α-ketoglutarate, 0.25 mM NAD^+, 0.2 mM TPP, 15 mU/100 μl KDH, 34 μM ACP, 25 μM malonyl-CoA, and 1.5 nM of SpMCAT or corresponding mutants.

2.5. Stoichiometric intermediate capture assay (SICA)

In order to test the effect of key residues of SpMCAT on the first step of the reaction, the relative activity of mutants versus wild type of spMCAT in forming malonyl-enzyme intermediate were determined. In SICA the procedure is modified by increasing the concentration of SpMCAT to 3 μM instead of 1.5 nM and replacing ACP by the corresponding buffer based on the coupled enzymatic assay mentioned above.

3. Results and discussion

3.1. Overall structure of MCAT

The crystal structure of SpMCAT was determined in space group $P2_12_12$ by molecular replacement using the *E. coli* MCAT (PDB: 1MLA) as initial model and refined at a resolution of 2.42 Å to an R_{free} of 25.6. The crystallographic statistics for data collection and structure refinement were summarized in Supplementary Table 2. All atoms were defined in the electron density maps suggesting a compact folding. As shown in Fig. 1A, the overall structure of SpMCAT was formed by two subdomains. The small domain was consisted of two helices and four antiparallel β-strands referring to residues 127–184. The large domain was composed of 11 helices surrounding a core of four parallel β-strands, involving residues 1–126 and 185–293.

The structure of SpMCAT contained no substrates, however, considering the sodium acetate in the crystallization reservoir, weak densities of a single acetate molecule bound to SpMCAT active site in a manner of mimicking the carboxyl end of the substrate malonyl-CoA could be observed which was in agreement with the structure of *S. pneumoniae* MCAT [8]. Visualizing the acetate molecule as malonyl-CoA, the substrate binding pocket was thoroughly defined and the residues involved in the reaction were shown in Fig. 1B. Acetate interacted with the NH1 atom of Arg113 at a distance of 3.1 Å, and was also stabilized by a hydrogen bond between the OG atom of Ser88 (2.8 Å). Additionally, the acetate was further stabilized by hydrophobic interactions with Gln10, Phe187 and Met117.

The active site was located in the cleft between the small and large subdomains. Key catalytic sites including the side chains of Ser88, His188 and Arg113 formed a catalytic triad. The catalytic Ser88 residue positioned in the apex of nucleophilic elbow between β2 and α5, and His188 stranded on a loop between β6 and α9, while Arg113 located on the α6 and formed hydrogen bond with Ser88. Previously Arg113 was not denoted as the catalytic residue, here however it indeed participates in the catalytic reaction by interaction with Ser88 and the substrate as well, which was further demonstrated from the biochemistry data below showing that R113A lost the activity without globe conformation change (unpublished Circular Dichroism data). Additionally, the backbone amides of Gln10 and Leu89 participated in the oxyanion hole formation by stabilizing the tetrahedral intermediate MCAT-malonyl-CoA and ACP-MCAT-malonyl as well. Met117 and Phe187 protruded inside of the binding pocket and stabilized the substrate through hydrophobic interactions.

3.2. Sequence and structure comparison of MCATs

By sequence alignment analysis of MCATs from multiple species, it is found that key catalytic residues are strictly conserved (Fig. 2A). Consistent with other typical α/β hydrolases, MCAT comprises the highly conserved serine in the GXSXG nucleophilic elbow and its hydroxyl group interacts with NE2 of His188 and NH2 of Arg113 by forming hydrogen bonds. In most cases of MCAT, the second X is histidine and functioned as a tetrahedral intermediate stabilizing factor [23], while the fourth X is determined by the substrate specificity of the serine protease [24]. It is worth pointing that another highly conserved pentapeptide GQGSQ motif which positioned in the N-terminal residues opposite the substrate binding site may play potential roles in activating the oxy anion hole and initiating the bond formation with the malonyl and the arm of the holo ACP [11]. To a certain extent, these similar regions elaborate the high level of evolutionary conservation of this essential enzyme.

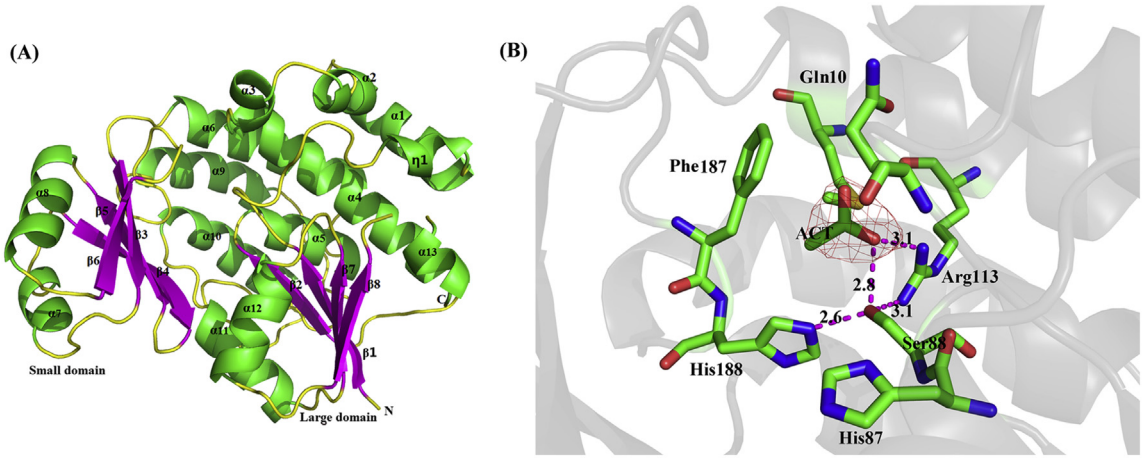

Fig. 1. Structural characterization of SpMCAT. (A) The Overall structure of SpMCAT. SpMCAT was composed of a small domain and a large domain, with α-helices and β-sheets shown in green and magenta, respectively, (B) Acetate molecular as a mimic substrate binding with SpMCAT. The 2Fo-Fc map contoured at 1.0σ. The hydrogen bonds were shown in magenta dotted lines and distance was represented in angstrom; critical residues participated in the interaction were shown in stick and colored by elements (carbon, green; nitrogen, blue; oxygen, red).(For interpretation of the references to colour in this figure legend, the reader is referred to the web version of this article.)

Several MCAT structures from species have been determined [9–12]. Sequence alignment showed that SpMCAT shared 39%, 37%, 33% and 28% identity with MCAT from *E. coli*, *M. tuberculosis*, *S. coelicolor* and *X. oryzae* in primary sequence, respectively. Furthermore, the three-dimensional structures of these proteins were superimposable, with a 1.0 Å root-mean-square (RMS) deviation considering 234 C_α-atom with *E. coli* MCAT. However, there still retained subtle differences especially represented in nonconservative sequence, such as η1 and α3 from SpMCAT being shifted outwards corresponding to EcMCAT (Fig. 2B).

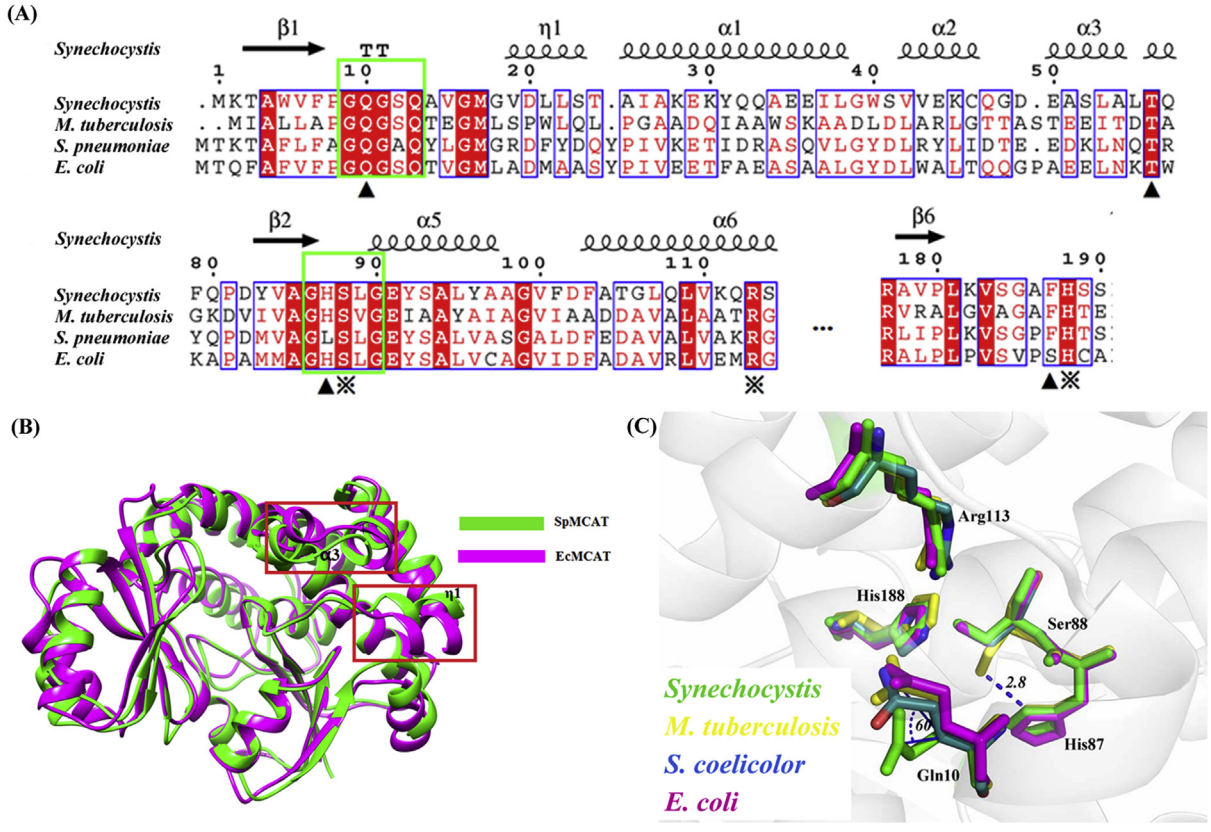

Fig. 2. Sequence, structure and active site comparison of MCATs. (A) Multiple sequence alignment of MCATs from four species. Asterisk indicated the Ser-His-Arg catalytic triad and closed triangle indicated the residual mutants in this study. The nucleophilic elbow and oxyanion hole motif were trapped by green rectangles. Structure and sequence alignment were performed using ESPript. (B) Structure comparison of SpMCAT (PDB: 4RR5) with EcMCAT from *E. coli* (PDB: 1MLA). The SpMCAT and EcMCAT were shown in green and magenta respectively, and the differences were shown in the red box. (C) Alignment of active sites of SpMCAT with EcMCAT (PDB: 1MLA), SpnMCAT from *S. coelicolor* (PDB: 1NM2) and MtMCAT from M. tuberculosis (PDB: 2QJ3). The active sites of SpMCAT, EcMCAT, MtMCAT and SpnMCAT were shown in green, magenta, yellow and blue, respectively. (For interpretation of the references to colour in this figure legend, the reader is referred to the web version of this article.)

3.3. Catalytic mechanism of SpMCAT

According to the documented information of the reaction catalyzed by MCAT and the crystal structure, the reaction mechanism is proposed in Fig. 3. Initially, the malonyl-CoA binds to MCAT, involving Ser88, Arg113, Met117 and Phe187; subsequently, NE2 atom of His188 extracts a proton from Ser88 OG by hydrogen bond and turns it into an active nucleophile. In the following, deprotonated hydroxyl group of Ser88 attacks the thioester carbonyl, and simultaneously a subtle conformational change of the enzyme occurs, resulting in the malonyl moiety forming as a tetrahedral intermediate stabilized by the oxyanion hole involving the backbone amide nitrogens of Leu89 and Gln10, the latter which furthermore interacts with Thr56 patterned by hydrogen bond. Malonyl-MCAT by C–O-Ser88 was formed with the release of CoA (step 1). In the second step, ACP approaches and its thiol of 4′-phosphopantetheine arm as nucleophilic reagent stretches into the carbon in the carbonyl of malonyl-Ser88 and again the malonyl moiety forms a tetrahedral intermediate with holo-ACP. The consequence is malonyl-ACP formation with MCAT release (step 2) while His188 NE2 atom protonates the catalytic serine as initial status.

3.4. Mutagenesis analysis of SpMCAT

Despite the highly conserved primary sequence in MCATs, they have different catalytic mechanisms which may result from different tertiary structures. According to published reports, the catalytic mechanism of MCAT was currently divided into three categories mainly. The first one is referring to Fig. 3 in which Ser88-His188 conducts proton transfer. The second one considered the active serine hydroxyl turning towards the neighboring histidine, hence the corresponding His87 substituting His188 to participate in the deprotonation represented in *M. tuberculosis* [10]. The third one is described in *S. coelicolor*, in which as an alternative mechanism, especially when Ser88-His188 interaction was inhibited, His87 acts as a nucleophilic candidate instead of Ser88 and cooperates with Asn152 by forming hydrogen bond to initialize the reaction [9]. All the mechanisms are related to the initializing of the reaction at the first step. Little information is available on the second step.

In order to identify the stepwise catalytic mechanism in *Synechocystis* sp. PCC 6803, mutagenesis and enzyme activity experiments were carried out. These mutations were classified into three groups. The first group was composed of residues Ser88, His188 and Arg113, which existed as central catalytic sites. As expected, R113A and H188A completely lost activities compared with the wild type enzyme (Fig. 4A). Unconventionally, the S88T mutant retained most of the enzyme activity by 90.7%. Considering the steric interference of the extra methyl group in threonine, in most cases, the serine mutation would substantially decrease the activity of the enzyme. While excluding conformation and bulk, there were no significant chemical differences between the OG atoms of threonine and serine residues [25]. Catalytic threonine residues have been identified in a few hydrolytic enzymes [26–28]. Here, through hydroxyl conformation simulation, we found that S88T hydroxyl adopted a more conducive orientation in which hydrogen bond with His87 was formed, functioning on initializing the reaction to substitute the Ser88-His188 catalytic mechanism, which happens in *M. tuberculosis* as the second catalytic mechanism of MCAT mentioned above. It may be a potential characteristic of MCAT, at least embodied in *Synechocystis* sp. PCC 6803.

The second mutagenesis group referred to Gln10 which was considered to form the oxyanion hole for stabilization of tetrahedral intermediates of step 1 and step 2. However, the activity of Q10A mutant declined to 26.6%, whereas that was observed to 10% or even lower from *Streptomyces* and *Mycobaterium* [10]. Detailed analysis of the tertiary structure showed that the side chain of Gln10 directed upwards of the backbone and flipped 60° comparing with MCAT from other species (Fig. 2C), revealing that the oxyanion hole of SpMCAT performed while only made a weak contribution in the intermediate step, which may be affected by its side chain deposition (Fig. 2C).

The third group contained residues Thr56 and Phe187, which were conservatively located at the entrance of the enzyme and participated in the reaction indirectly. The T56A mutant declined to a 34% activity, indicating its role in hydrogen-bond interaction with

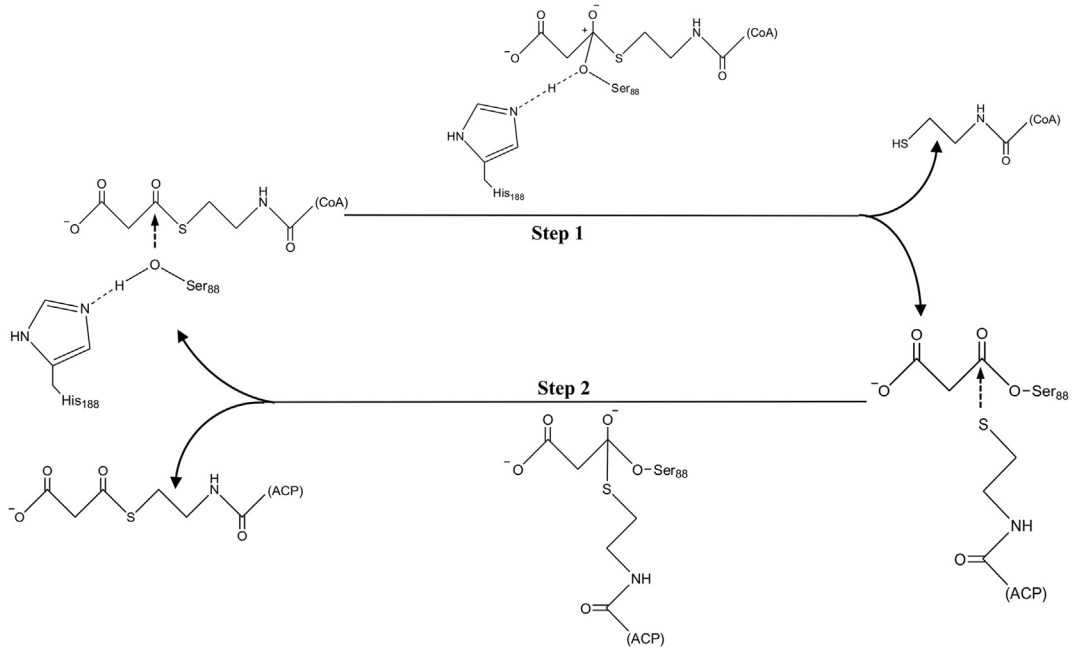

Fig. 3. Catalytic mechanism of SpMCAT.

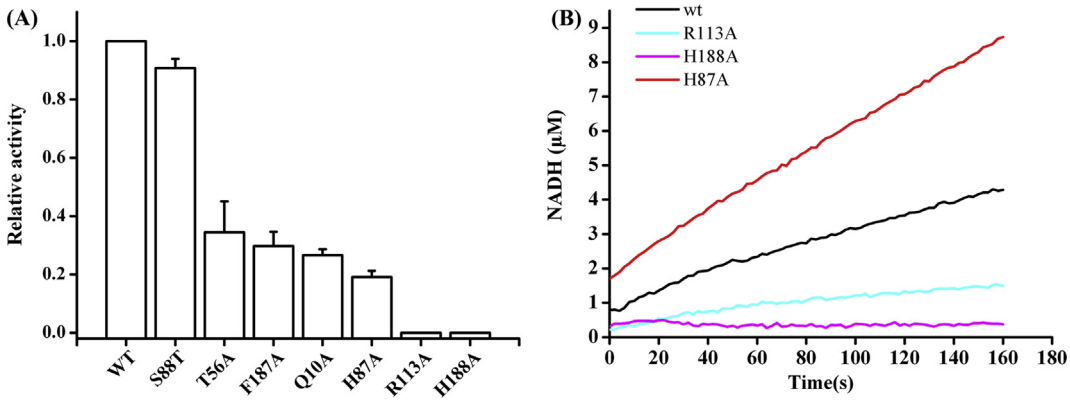

Fig. 4. Enzymatic activity and stoichiometric intermediate capture assay of wide-type SpMCAT and mutants. (A) Relative activities of SpMCAT mutants measured with ACP present in the reaction mixture; (B) Kinetic analysis of stoichiometric intermediate capture assay from wide-type SpMCAT and mutants.

Gln10. Furthermore, originally as a substrate hydrophobic interaction stabilizing factor, the F187A mutant reduced the activity to 29.7% comparing with the wild type, further assuring the previous study that this phenylalanine acts as a selective filter [29].

3.5. Determination of the MCAT speed-limited step

So far, MCAT researches mainly focused on the first step (Fig. 3), referring to the first tetrahedral intermediate formation and coenzyme A release, and the entire reaction. However, the second step, involving holo-ACP approach and malonyl-ACP produce was not clear. For the first step, C—O bond is formed by C—S bond cleavage, while in the second step the manner is reversed with C—S bond formation by C—O bond cleavage. To stabilize the tetrahedral intermediates in the individual step the residues involved should be different because the first step is exergonic and the second step is endergonic. Considering the products of coenzyme A and MCAT-malonyl in the first step, SICA was performed to examine the first step without ACP in the reaction system. MCAT-malonyl intermediate was not stable and tended to hydrolyze after 2 min in the reaction [29]. Here we tried to conduct the experiment in a reasonable linear range (Fig. 4B), so as to disregard the influence of the hydrolysis. As a negative control, the H188A mutant indeed was inactive, indicating its proton transfer role in initializing the reaction.

Surprisingly, an increased enzyme activity was observed in H87A mutant compared to the wild type one. Actually it was possible that His87 located at the entrance of the binding pocket and the mutant made the access of substrate to the binding pocket in a more unconstrained style. Together with 19.1% overall relative activity of the H87A enzyme, it was deduced that His87 mostly assists stabilizing of the MCAT-malonyl-ACP tetrahedral intermediate, or participate in deprotonating thiol of 4′-phosphopantetheine arm of ACP in the second step while contributes less in the first step. Moreover, in the reaction system without ACP, the R113A mutant remained part of its activity, while it was completely inoperative in the overall enzymatic proceeding. Both of these results demonstrated that the second intermediate ACP-MCAT-malonyl formation and malonyl-ACP release were crucial and speed-limited in the catalysis process, consistent with the notion that the cleavage of C—O bond to generate C—S bond in the second step reaction needs more energy. It has suggesteded different enzymatic conformational changes from the two steps. The detailed information about it is still a mystery.

In conclusion, the structure of MCAT from *Synechocystis* sp. PCC 6803 was determined at 2.42 Å resolution. Through ligand simulation and structural analysis, the Ser88- His188-Arg113 catalytic triad was presented. On the basis of further mutagenesis validation, a distinct S88T mutant was determined, indicating another unconventional catalytic mode, meanwhile, a relatively conserved His87 was identified, which played an extraordinary role in the second tetrahedral intermediate formation process. The second step of Malonyl-coenzyme A: acyl-carrier protein transacylation is the speed-limited step in which most highly conserved residues play important roles rather than in the first step. The results provided detailed insights into the catalytic mechanism of MCAT from cyanobacteria which was useful to further understand the fatty acid synthesis in photosynthetic microorganisms.

Conflict of interest

There is no conflict of interest.

Acknowledgments

We cordially thank the staff of beamline BL17U1 at the Shanghai Synchrotron Radiation Facility, People's Republic of China for assistance in synchrotron X-ray data collection. We appreciate Professor Tiangang Liu (Wuhan University) for kindly providing the host strain BAP1 for holo-ACP expression. This study was supported by the National Key Basic Research Program of China‘973 Program’ (2011CBA00803) and the Hundred Talents Program of the Chinese Academy of Sciences (grant No. A1097).

Appendix A. Supplementary data

Supplementary data related to this article can be found at http://dx.doi.org/10.1016/j.bbrc.2015.01.003.

References

[1] F.E. Ruch, P.R. Vagelos, Isolation and general properties of *Escherichia coli* malonyl coenzyme-a-acyl carrier protein transacylase, J. Biol. Chem. 248 (1973) 8086–8094.
[2] W.Z. Liu, C. Han, L.H. Hu, K.X. Chen, X. Shen, H.L. Jiang, Characterization and inhibitor discovery of one novel malonyl-CoA: acyl carrier protein transacylase (MCAT) from *Helicobacter pylori*, FEBS Lett. 580 (2006) 697–702.
[3] D.C. Ducat, J.C. Way, P.A. Silver, Engineering cyanobacteria to generate high-value products, Trends Biotechnol. 29 (2011) 95–103.
[4] I.M.P. Machado, S. Atsumi, Cyanobacterial biofuel production, J. Biotechnol. 162 (2012) 50–56.
[5] A. Parmar, N.K. Singh, A. Pandey, E. Gnansounou, D. Madamwar, Cyanobacteria and microalgae: a positive prospect for biofuels,, Bioresour. Technol. 102 (2011) 10163–10172.
[6] G. Bonaventure, J.B. Ohlrogge, Differential regulation of mRNA levels of acyl carrier protein isoforms in Arabidopsis, Plant Physiol. 128 (2002) 223–235.

[7] V.S. Eccleston, J.B. Ohlrogge, Expression of lauroyl-acyl carrier protein thioesterase in *Brassica napus* seeds induces pathways for both fatty acid oxidation and biosynthesis and implies a set point for triacylglycerol accumulation, Plant Cell. 10 (1998) 613–621.
[8] S.K. Hong, K.H. Kim, J.K. Park, K.-W. Jeong, Y. Kim, E.E. Kim, New design platform for malonyl-CoA-acyl carrier protein transacylase, FEBS Lett. 584 (2010) 1240–1244.
[9] A.T. Keatinge-Clay, A.A. Shelat, D.F. Savage, S.C. Tsai, L.J.W. Miercke, J.D. O'Connell, C. Khosla, R.M. Stroud, Catalysis, specificity, and ACP docking site of *Streptomyces coelicolor* malonyl-CoA : ACP transacylase, Structure 11 (2003) 147–154.
[10] Z. Li, Y. Huang, J. Ge, H. Fan, X. Zhou, S. Li, M. Bartlam, H. Wang, Z. Rao, The crystal structure of MCAT from *Mycobacterium tuberculosis* reveals three new catalytic models,, J. Mol. Biol. 371 (2007) 1075–1083.
[11] S. Natarajan, J.-K. Kim, T.-K. Jung, D. Thanh Thi Ngoc, N. Ho-Phuong-Thuy, M.-K. Hong, S. Kim, T. Viet Pham, S.J. Ahn, S.H. Lee, Y. Han, Y.-J. Ahn, L.-W. Kang, Crystal structure of malonyl CoA-Acyl carrier protein transacylase from *Xanthomanous oryzae* pv. *oryzae* and its proposed binding with ACP, Mol. Cells 33 (2012) 19–25.
[12] L. Serre, E.C. Verbree, Z. Dauter, A.R. Stuitje, Z.S. Derewenda, The *Escherichia coli* malonyl-coa-acyl carrier protein transacylase at 1.5-angstrom resolution - crystal-structure of a fatty-acid synthase component,, J. Biol. Chem. 270 (1995) 12961–12964.
[13] L. Zhang, W. Liu, J. Xiao, T. Hu, J. Chen, K. Chen, H. Jiang, X. Shen, Malonyl-CoA: acyl carrier protein transacylase from *Helicobacter pylori*: Crystal structure and its interaction with acyl carrier protein, Protein Sci. 16 (2007) 1184–1192.
[14] Y. Liu, Y. Zhang, X. Cao, S. Xue, Cloning, purification, crystallization and preliminary X-ray crystallographic analysis of MCAT from *Synechocystis* sp. PCC 6803, Acta Crystallogr. F. 69 (2013) 1256–1259.
[15] B.A. Pfeifer, S.J. Admiraal, H. Gramajo, D.E. Cane, C. Khosla, Biosynthesis of complex polyketides in a metabolically engineered strain of *E. coli*, Science 291 (2001) 1790–1792.
[16] A.J. McCoy, R.W. Grosse-Kunstleve, P.D. Adams, M.D. Winn, L.C. Storoni, R.J. Read, Phaser crystallographic software, J. Appl. Crystallogr. 40 (2007) 658–674.
[17] M.D. Winn, C.C. Ballard, K.D. Cowtan, E.J. Dodson, P. Emsley, P.R. Evans, R.M. Keegan, E.B. Krissinel, A.G.W. Leslie, A. McCoy, S.J. McNicholas, G.N. Murshudov, N.S. Pannu, E.A. Potterton, H.R. Powell, R.J. Read, A. Vagin, K.S. Wilson, Overview of the CCP4 suite and current developments, Acta Crystallogr. D. 67 (2011) 235–242.
[18] P.D. Adams, P.V. Afonine, G. Bunkoczi, V.B. Chen, I.W. Davis, N. Echols, J.J. Headd, L.W. Hung, G.J. Kapral, R.W. Grosse-Kunstleve, A.J. McCoy, N.W. Moriarty, R. Oeffner, R.J. Read, D.C. Richardson, J.S. Richardson, T.C. Terwilliger, P.H. Zwart, PHENIX: a comprehensive python-based system for macromolecular structure solution, Acta Crystallogr. D. 66 (2010) 213–221.
[19] P. Emsley, B. Lohkamp, W.G. Scott, K. Cowtan, Features and development of coot, Acta Crystallogr. D 66 (2010) 486–501.
[20] E.F. Pettersen, T.D. Goddard, C.C. Huang, G.S. Couch, D.M. Greenblatt, E.C. Meng, T.E. Ferrin, UCSF chimera-A visualization system for exploratory research and analysis, J. Comput. Chem. 25 (2004) 1605–1612.
[21] X. Robert, P. Gouet, Deciphering key features in protein structures with the new ENDscript server, Nucleic Acids Res. 42 (2014) W320–W324.
[22] J. Molnos, R. Gardiner, G.E. Dale, R. Lange, A continuous coupled enzyme assay for bacterial malonyl-CoA : acyl carrier protein transacylase (FabD), Anal. Biochem. 319 (2003) 171–176.
[23] S. Poust, I. Yoon, P.D. Adams, L. Katz, C.J. Petzold, J.D. Keasling, Understanding the role of histidine in the GHSxG Acyltransferase active site motif: Evidence for histidine stabilization of the malonyl-enzyme intermediate, PLoS One 9 (2014) e109421.
[24] S.F. Haydock, J.F. Aparicio, I. Molnar, T. Schwecke, L.E. Khaw, A. Konig, A.F.A. Marsden, I.S. Galloway, J. Staunton, P.F. Leadlay, Divergent sequence motifs correlated with the substrate-specificity of (methyl)malonyl-coa-acyl carrier protein transacylase domains in modular polyketide syntheses, FEBS Lett. 374 (1995) 246–248.
[25] G. Dodson, A. Wlodawer, Catalytic triads and their relatives, Trends. Biochem. Sci. 23 (1998) 347–352.
[26] J. Lowe, D. Stock, R. Jap, P. Zwickl, W. Baumeister, R. Huber, Crystal-structure of the 20s proteasome from the Archaeon *T. acidophilum* at 3.4-angstrom resolution, Science 268 (1995) 533–539.
[27] C. Oinonen, R. Tikkanen, J. Rouvinen, L. Peltonen, 3-Dimensional structure of human lysosomal aspartylglucosaminidase, Nat. Struct. Biol. 2 (1995) 1102–1108.
[28] R. Zhang, G. Zhu, W. Zhang, S. Cao, X. Ou, X. Li, M. Bartlam, Y. Xu, X.C. Zhang, Z. Rao, Crystal structure of a carbonyl reductase from *Candida parapsilosis* with anti-Prelog stereospecificity, Protein Sci. 17 (2008) 1412–1423.
[29] A.T. Koppisch, C. Khosla, Structure-based mutagenesis of the Malonyl-CoA : acyl carrier protein transacylase from *Streptomyces coelicolor*, Biochemistry 42 (2003) 11057–11064.